

## Ammonia reduced graphene oxides as a hole injection layer for CdSe/CdS/ZnS quantum dot light-emitting diodes

This content has been downloaded from IOPscience. Please scroll down to see the full text.

2016 Nanotechnology 27 325201

(<http://iopscience.iop.org/0957-4484/27/32/325201>)

View [the table of contents for this issue](#), or go to the [journal homepage](#) for more

Download details:

IP Address: 159.226.165.17

This content was downloaded on 02/07/2017 at 10:21

Please note that [terms and conditions apply](#).

You may also be interested in:

[Efficient quantum dot light-emitting diodes with solution-processable molybdenum oxide as the anode buffer layer](#)

Shaojian He, Shusheng Li, Fuzhi Wang et al.

[Single layer graphene electrodes for quantum dot light emitting diodes](#)

Long Yan, Yu Zhang, Xiaoyu Zhang et al.

[Improved electroluminescence of quantum dot light-emitting diodes enabled by a partial ligand exchange with benzenethiol](#)

Daekyoung Kim, Yan Fu, Jungwoo Kim et al.

[Solution-Processed White Light-Emitting Diode Utilizing Hybrid Polymer and Red–Green–Blue Quantum Dots](#)

Byoung Wook Kwon, Dong Ick Son, Dong-Hee Park et al.

[Luminance enhancement in quantum dot light-emitting diodes fabricated with Field's metal as the cathode](#)

Carlos Basilio, Jorge Oliva, Tzarara Lopez-Luke et al.

[Efficient and stable polymer solar cells prepared using plasmonic graphene oxides as anode buffers](#)

Chung-Lei Chen, Ming-Kai Chuang, Chyong-Hua Chen et al.

[Effect of anode buffer layer on the efficiency of inverted quantum-dot light-emitting diodes](#)

Ye Ram Cho, Pil-Gu Kang, Dong Heon Shin et al.

[Single active-layer structured dual-function devices using hybrid polymer–quantumdots](#)

Dong-Ick Son, Dong-Hee Park, Sang-Yub Je et al.

# Ammonia reduced graphene oxides as a hole injection layer for CdSe/CdS/ZnS quantum dot light-emitting diodes

Qing Lou<sup>1</sup>, Wen-Yu Ji<sup>2</sup>, Jia-Long Zhao<sup>3</sup> and Chong-Xin Shan<sup>1,2</sup>

<sup>1</sup> School of Physical Engineering, Zhengzhou University, Zhengzhou 450052, People's Republic of China

<sup>2</sup> State Key Laboratory of Luminescence and Applications, Changchun Institute of Optics, Fine Mechanics and Physics, Chinese Academy of Sciences, Changchun, 130033, People's Republic of China

<sup>3</sup> Key Laboratory of Functional Materials Physics and Chemistry of the Ministry of Education, Jilin Normal University, Siping 136000, People's Republic of China

E-mail: [jiwy@ciomp.ac.cn](mailto:jiwy@ciomp.ac.cn) and [shancx@ciomp.ac.cn](mailto:shancx@ciomp.ac.cn)

Received 14 January 2016, revised 14 May 2016

Accepted for publication 24 May 2016

Published 27 June 2016



CrossMark

## Abstract

In this study, we report quantum-dot light-emitting devices (QD-LEDs) using ammonia reduced graphene oxide (rGO) as a hole injection layer (HIL). Compared with pristine GO, QD-LEDs employing rGO as a HIL show higher maximum luminance ( $936 \text{ cd m}^{-2}$  versus  $699 \text{ cd m}^{-2}$ ) and lower turn-on voltage ( $V_{\text{th}}$ , 5.0 V versus 7.5 V). The improved performance can be attributed to the synergistic effect of the improved conductivity ( $1.27 \mu\text{S cm}^{-1}$  versus  $0.139 \mu\text{S cm}^{-1}$ ) and decreased work function (5.27 eV versus 5.40 eV) of the GO after the reduction process. The above results indicate that ammonia functionalized graphene may be a promising hole injection material for QD-LEDs.

 Online supplementary data available from [stacks.iop.org/NANO/27/325201/mmedia](http://stacks.iop.org/NANO/27/325201/mmedia)

Keywords: graphene oxide, hole injection layer, quantum dot, light emitting diodes

(Some figures may appear in colour only in the online journal)

## 1. Introduction

In recent years, colloidal II-VI semiconductor quantum dots (QDs) have received considerable attention for their applications in full-color displays and low-cost solid state lighting [1–6]. QD-based light-emitting diodes (QD-LEDs) have manifested many unique advantages in optoelectronic devices such as narrow emission bandwidth, wide emission spectral window in the visible region, and low cost and large area manufacturing based on solution processes [7, 8]. To date, enormous strides have been made to optimize the performance of QD-LEDs through many approaches, such as developing efficient and stable QD and transport materials, designing novel device architecture, and exploring the essential device physics [2, 8–11]. However, improving the electroluminescence (EL) performance is still one of the most important issues for QD-LEDs.

So far, the most widely used device structure of QD-LEDs is composed of a thin layer of luminescent QDs sandwiched between organic or inorganic hole and electron injection/transport layers. The proper selection of charge injection/transport layers is an important issue that determines the performance of QD-LEDs because the existence of these layers in QD-LEDs can balance electron and hole injection into a QD layer, reduce the contact barrier between the indium tin oxide (ITO) electrode and the active QD layers, and enhance the stability of device performance [12–14]. Various hole injection layers (HILs), including organic molecular materials and wide band gap p-type inorganic materials, have been introduced to improve the hole injection and transport path towards the radiative recombination zone in the QD layer. Water-soluble poly(styrenesulfonate)-doped poly(3,4-ethylenedioxythiophene) (PEDOT:PSS), the most commonly used as a solution-processable HIL in light-emitting devices, can effectively reduce the ITO roughness upon

spin-coating and improve the contact property between active layer and transparent anode [15]. However, PEDOT:PSS can gradually corrode the ITO electrode and eventually deteriorate the long-term stability and performance of the device because of its highly acidic nature ( $\text{pH} \sim 1$ ), and hygroscopic properties in the presence of moisture [16, 17]. Recently, stable and nonacidic metal oxides such as molybdenum oxide ( $\text{MoO}_3$ ), tungsten oxide ( $\text{WO}_3$ ), and nickel oxide ( $\text{NiO}_x$ ) have been employed as HILs [18–20]. However, cost-intensive deposition techniques such as vacuum systems or high temperature annealing are usually needed to deposit such materials, which is incompatible with solution-processed optoelectronic devices. Therefore, simply processable and efficient hole-injecting materials have been highly desired. Graphene oxide (GO), consisting of epoxy and hydroxyl groups on the graphene sheet basal plane and carboxylic groups at the edges, contains a mixture of  $\text{sp}^2$ - and  $\text{sp}^3$ -hybridized carbon atoms. The  $\text{sp}^3$ -hybridized carbon atoms on the basal plane can disrupt the conjugation of the hexagonally  $\text{sp}^2$ -bonded graphene lattice to render GO an insulator or semiconductor. It is feasible to tune the optical and electronic properties of GO through manipulating the size, shape and relative fraction of the  $\text{sp}^2$ -hybridized domains of GO or functionalizing GO with other groups or metal ions. Recently, solution-processed GO and its derivatives have been widely studied as charge transport/injection layers for various optoelectronic devices such as organic solar cells (OSCs), light-emitting devices (LEDs), etc [21–25]. However, GO films are usually functionalized by a highly toxic and explosive hydrazine reagent for optimizing device performance. Meanwhile, it is difficult to eliminate irreversible aggregation during the reduction process with hydrazine. Furthermore, reduced GO (rGO) fabricated by using hydrazine has a dispersion concentration as low as  $0.3 \text{ mg ml}^{-1}$  or lower, which is detrimental to their practical applications [24]. Therefore, it is necessary to find new reduction methods using nontoxic chemicals to produce appropriate rGOs, which keep a suitable electron-blocking, hole injection and conductivity behavior.

Recently, for the first time, Wang *et al* employed GO as the anode interfacial layer to fabricate QD-LEDs, but the maximum luminance ( $165 \text{ cd m}^{-2}$ ) and external quantum efficiency (0.08%) of the device still are very low and need to be investigated more deeply [25]. Based on their initial work, we adopt GOs reduced by ammonia as the HIL for QD-LEDs. The GO film possesses two important advantages: (1) it has simply tunable optical and electronic properties, which provide a robust platform for independently optimizing the charge injection and charge carrier confinement in the QDs and (2) excellent physical and chemical stability, which is beneficial to operational lifetime of devices. To improve device performance using GO as a HIL, it is usually necessary to tune its optical and electronic properties, for which ammonia has been used to reduce the GO. As a result, the performance of the prepared devices was much more improved than the previous study ( $936 \text{ cd m}^{-2}$ ). We observed a decrease in the conductivity and uplift in the Fermi level in the devices with prolonged reduction time. Correspondingly,

the maximum luminance of the devices has been enhanced by 134% with a 1 h ammonia-reduced GO interlayer. The improved performance of devices can be attributed to the synergic effect of carrier transport and charge injection, which means that GO film has great potential to be used in QD-LEDs as charge injection layers.

## 2. Experimental details

### 2.1. Preparation of CdSe/CdS/ZnS QDs

CdSe/CdS/ZnS QDs were prepared according to the method reported in the literature [10, 11].

### 2.2. Synthesis of GO with ammonia reduction (rGO)

Graphene oxide (GO) was purchased from Nanjing XFNANO Materials Tech Co., Ltd. Typically, ammonia ( $35 \mu\text{l}$ , 28 wt % in water) was added to the GO aqueous suspension ( $10 \text{ ml}$ ,  $0.5 \text{ mg ml}^{-1}$ ). The mixture was kept in a tightly sealed glass vial and heated to  $95 \text{ }^\circ\text{C}$  under magnetic stirring for 1, 3 and 6 h, respectively. Then, the solution was centrifuged at 7200 rpm, and the obtained black slurry was washed with deionized water several times. The as-prepared rGO was dissolved in a solvent mixture of water/ethanol = 1/1 ( $1 \text{ mg ml}^{-1}$ ). Then, the films of rGO for conductivity test were prepared by negative-pressure filtration and dried in air.

### 2.3. Fabrication of QD-LEDs

The QD-LEDs consist of ITO/GO or rGO (5 nm)/poly (*N,N'*-bis(4-butylphenyl)-*N,N'*-bis(phenyl)-benzidine) (poly-TPD,  $\sim 40 \text{ nm}$ )/QDs (25 nm)/2,2',2''-(1,3,5-benzinetriyl)-tris(1-phenyl-1-*H*-benzimidazole) (TPBi, 55 nm)/lithium fluoride (LiF,  $\sim 1 \text{ nm}$ )/aluminum (Al, 100 nm). The GO/rGO, poly-TPD, QDs, TPBi and LiF are used as HIL, hole transport layer (HTL), emission layer, electron transport layer (ETL), and electron injection layer (EIL), respectively. The ammonia-reduction time of GO layer is varied from 0 h to 6 h for different devices: device A (0 h), device B (1 h), device C (3 h), and device D (6 h). Device A is a control device with GO as the HIL without ammonia reduction. All the devices were fabricated on patterned ITO glass substrates (sheet resistance,  $15 \Omega \text{ sq}^{-1}$ ), which had been successively cleaned by ultrasonic in acetone, ethanol, deionized water, isopropanol, and then dried under a  $\text{N}_2$  stream. The GO/rGO solutions (in a solvent mixture of water/ethanol,  $1 \text{ mg ml}^{-1}$ ) were spin-coated onto the cleaned ITO substrates at 2000 rpm for 60 s and baked at  $120 \text{ }^\circ\text{C}$  for 15 min, and the spin-coating process was repeated twice to obtain a desired full coverage on ITO substrates by the GO/rGO. The GO/rGO-coated substrates were transferred into a nitrogen-filled glove box (MBRAUN) and poly-TPD (in chlorobenzene,  $10 \text{ mg ml}^{-1}$ ), QDs (in toluene,  $5 \text{ mg ml}^{-1}$ ) was deposited layer by layer by spin-coating at 2000 rpm for 60 s. The poly-TPD and QD layers were baked at  $110 \text{ }^\circ\text{C}$  for 40 min and at  $70 \text{ }^\circ\text{C}$  for 30 min, respectively, before the deposition of the next layer.

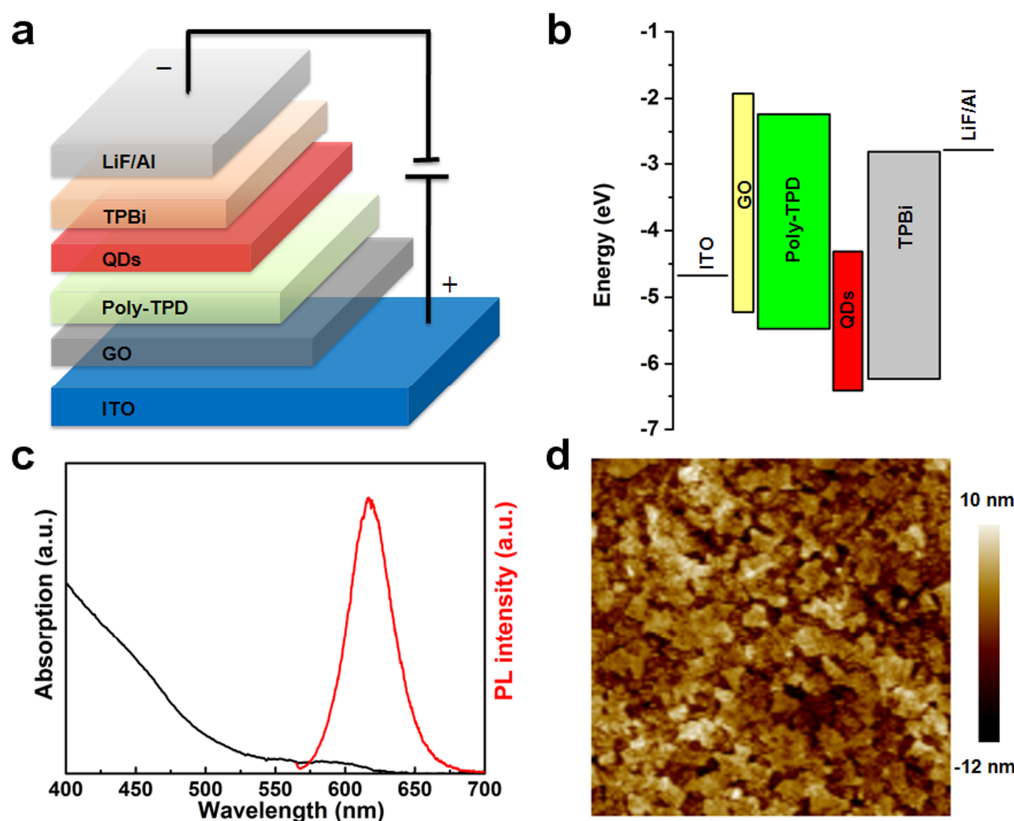


**Figure 1.** (a) Schematic structure and flat-band energy level diagram (b) of the QD-LEDs. (c) The absorption and PL spectra of the QDs used in our work. (d) AFM image of the GO film coated on ITO glass.

The substrates were then quickly loaded into the vacuum chamber and the rest of device fabrication was finished under a vacuum of  $\sim 4 \times 10^{-6}$  Torr. The active area of the device was  $5 \text{ mm}^2$  as defined by the overlapping area of the ITO and Al electrodes. TPBi was purchased from LumTec and poly-TPD was purchased from American Dye Source. All the materials were used as received without any further purification.

#### 2.4. Characterizations

The EL characteristics of the QD-LEDs were cross-checked using a system comprising a photometer (Minolta Luminance Meter LS-110) coupled with a computer-controlled Keithley 2400 power supply in air without any encapsulation. The EL spectra of the devices were obtained through a Ocean Optics Maya 2000-PRO spectrometer coupled with a Keithley 2400 power source. The thicknesses of the GO, rGO, poly-TPD, and QD layer were obtained using a Dektak 6 M stylus profilometer. The surface morphology of the GO layer was characterized by a Bruker Multimode-8 atomic force microscope (AFM) and a Hitachi S-4800 field emission scanning electron microscope (SEM). Transmission electron microscopy (TEM) images were recorded with a FEI-TECNAI G2 F30 transmission electron microscope operating at 200 kV for CdSe/CdS/ZnS QDs. Ultraviolet-visible absorption spectra of the QDs were collected using a Shimadzu UV-3101PC spectrophotometer. Fluorescence spectra of the LEDs were

recorded on a Hitachi F-7000 spectrometer. FT-IR measurements were performed with a Perkin-Elmer spectrometer (Spectrum One B). The conductivity test was carried out using a Victor VC890D digital multimeter (ShenZhen, PR China). Ultraviolet photoelectron spectroscopy (UPS) spectra were recorded on an ESCALAB MK II x-ray photoelectron spectrometer with a He I (21.2 eV) gas discharge lamp. Photoluminescence quantum yields were obtained in a calibrated integrating sphere in FLS920 spectrometer.

### 3. Results and discussion

The device structure (figure 1(a)) we employed is given as multiple layers of ITO, GO, poly-TPD, CdSe/CdS/ZnS QDs, TPBi, LiF, Al. The CdSe/CdS/ZnS core-shell QDs prepared according to our previous reports are used as the active layer of the device [10, 11]. The poly-TPD and TPBi layers are employed as the hole transport layer and electron transport layer, respectively. The GO layer deposited on ITO by a spin-coating process, acts as hole injection layer sandwiched between ITO and the organic semiconductors (poly-TPD). Due to the existence of  $\text{sp}^3$ -hybridized carbon atoms on the basal plane disrupting the conjugation of the  $\text{sp}^2$ -bonded graphene lattice, GO behaves as an insulator with a large band gap of around 3.6 eV. Considering the energy level alignment (figure 1(b)) of the device, GO performs a lower work function (WF,  $\sim 5.2$  eV) compared to ITO film ( $\sim 4.6$  eV),

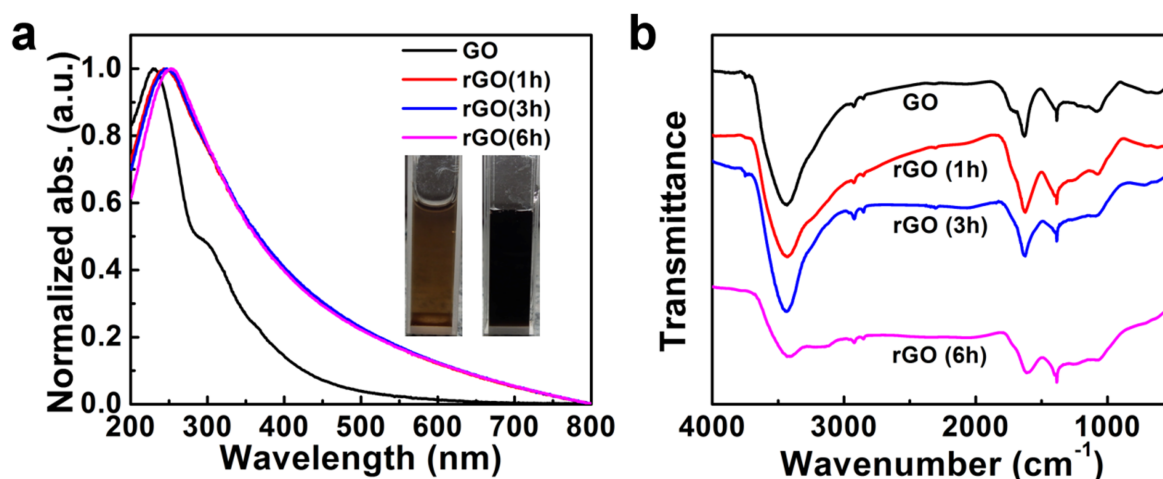


**Figure 2.** The absorption (a) and FT-IR (b) spectra of the pristine GO and GO with ammonia reduction time of 1 h, 3 h, and 6 h. The inset of (a) shows the image of the pristine GO (left) and GO after ammonia reduction for 1 h (right).

which could produce efficient hole injection from ITO to the highest occupied molecular orbital (HOMO) level of poly-TPD [25]. In our case, the introduction of GO will lower the Fermi level of the ITO anode in the device, leading to the diminution of energy barrier for the injection of holes from ITO to the HOMO level of the poly-TPD, thus holes can be injected into the QDs more efficiently. Figure 1(c) illustrates the absorption and PL spectra of CdSe/CdS/ZnS QDs (in toluene). The PL spectrum has a narrow full width at half-maximum (FWHM) of 35 nm peaked at 617 nm, and the QDs show a quantum yield of ~60%. The transmission electron microscopy (TEM) image shows that the QD has an average diameter of ~8.0 nm with high crystallinity (supplementary figure S1, [stacks.iop.org/NANO/27/325201/mmedia](http://stacks.iop.org/NANO/27/325201/mmedia)). The atomic force microscopy (AFM) image of the close-packed thin film of GO sheets ranging from 1 to 10  $\mu\text{m}$  on ITO is shown in figure 1(d). The root mean square roughness (RMS) of the GO layer is 3.21 nm, indicating that the layer has a smooth surface, which is important for the device performance.

Although the introduction of GO can realize efficient hole injection into the QD layers, the relatively high resistivity and low hole mobility of the GO hinder the achievement of low turn-on voltage ( $V_{\text{th}}$ , the voltage of device at the luminance of  $1 \text{ cd m}^{-2}$ ) and high power efficiency in the device. Therefore, the key component of this device is the realization of fine-modulating the optical and electronic properties of the GO. In this study, ammonia was employed as a reductant to optimize the properties of GO to fulfill a moderate hole mobility in the device.

The reaction process of ammonia treatment on GO was monitored using UV-vis spectroscopy. As shown in figure 2(a), the C=C absorption peak of the GO dispersion around 230 nm gradually red-shifts to 260 nm with the increase of the reduction time, and the absorption in the whole spectral region ( $>230 \text{ nm}$ ) increases upon ammonia reduction, suggesting that  $\pi$ -electron concentration and structural ordering within the graphene sheets is increased. Correspondingly, the yellow-brown GO suspension finally turns

black after reaction with ammonia for 1 h at  $95^\circ\text{C}$ , suggesting that an efficient reduction of GO has taken place (the inset of figure 2(a)). The above results imply that the electronic conjugation level of the GO can be chemically controllable through ammonia reduction, offering possibilities to tailor the degree of reduction and electrical properties of GO. Meanwhile, it is evidenced from figure 2(a) that the reduced GO shows an absorption peak at longer wavelength, indicating that the bandgap of the GO has been decreased after the treatment [24, 25].

Figure 2(b) shows the typical FT-IR spectra of the GO after reduction by ammonia. For GO, the characteristic peaks for O-H stretching and deformation vibration appear at around  $3430 \text{ cm}^{-1}$  and  $1400 \text{ cm}^{-1}$ , and C=O stretching vibration at  $1720 \text{ cm}^{-1}$ . The peak located at  $1634 \text{ cm}^{-1}$  is associated with aromatic C=C stretching vibration, and the peak at  $1045 \text{ cm}^{-1}$  can be ascribed to the alkoxy C-O stretching vibration mode [26, 27]. After reduction by ammonia, the peaks for most oxygen-containing functional groups decrease gradually with increasing the reaction time, and some peaks disappear completely, revealing most oxygen functionalities in the GO have been removed. Meanwhile, the frame of  $\text{sp}^2$  carbon atoms within the graphene sheets is retained well after the reduction process, as indicated by the peak at around  $1634 \text{ cm}^{-1}$ . These findings indicate that the degree of reduction can be tuned by changing the reaction time. Note that the conductivity of the GO changes with ammonia reduction. The pristine GO film exhibits an average conductivity of  $0.139 \mu\text{S cm}^{-1}$  (table S1), while the conductivity of the GO films with 1 h, 3 h, and 6 h ammonia reduction are one order of magnitude higher,  $1.27 \mu\text{S cm}^{-1}$ ,  $1.791 \mu\text{S cm}^{-1}$  and  $3.97 \mu\text{S cm}^{-1}$ , respectively. It reveals that the conductivity of the GO has a moderate increase after the ammonia reduction process.

Figures 3(a) and (b) show SEM images of the GO films on ITO substrates. The number of spin-coated layers has a great influence on the morphology and thickness of the GO films (figures 3(a) and S2). The deposition of full-coverage GO films on ITO substrates is essential for reducing leakage

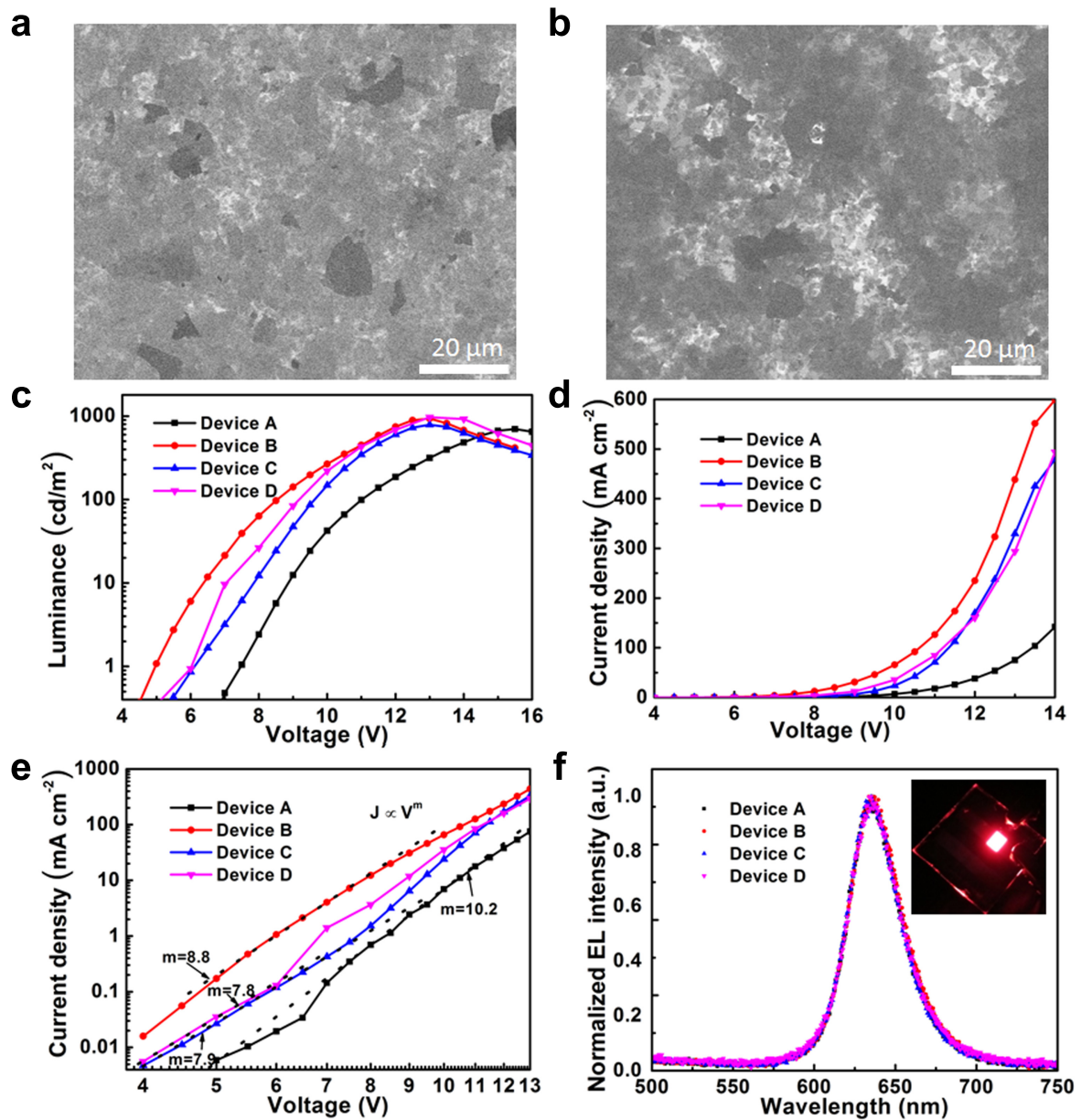


**Figure 3.** SEM images of the GO (a) and GO after 6 h ammonia reduction (b) with two spin-coated layers on ITO. (c) The luminance–voltage, (d) current density–voltage, and (e) current density–voltage on double-logarithmic axes characteristics of the QD-LEDs. (f) Normalized EL spectra of the QD-LEDs at an applied voltage of 10.0 V, and the inset represents the image of Device A under the operation voltage of 8.0 V.

current and constructing high-performance devices. Hence, it is necessary to repeat the spin-coating of GO and rGO, leading to the full coverage of GO and rGO films. The average thicknesses of the GO and rGO films were measured to be both approximately 5.0 nm by a stylus profilometer.

The device characteristics of the QD-LEDs with GO, and rGO (different reduction time) are presented in figure 3. Figure 3(c) shows that all the four devices exhibit similar luminance–voltage characteristics. The device with GO as a hole injection layer shows a maximum luminance of  $699 \text{ cd m}^{-2}$  (at 15.5 V). In contrast, the QD-LED with a rGO layer shows enhanced brightness and reduced drive voltage. The maximum luminance of the QD-LEDs using GO reduced by ammonia for 1 h, 3 h, and 6 h are  $936 \text{ cd m}^{-2}$ ,  $789 \text{ cd m}^{-2}$ ,

and  $969 \text{ cd m}^{-2}$  (at 13.0 V), which are enhanced by 134%, 113%, and 138%, respectively, compared to the devices with GO. Additionally, the  $V_{\text{th}}$  of all the rGO-containing devices is less than that of the control device with GO (7.5 V). The lowest  $V_{\text{th}}$  is obtained when the time of ammonia reduction on GO is 1 h for device B, which is increased from 5.0 to 6.0 V for device D with a 6 h ammonia reduction on the GO layer. Moreover, rGO-containing devices need a lower current density than GO-containing device to reach the peak efficiency, as more space charges for GO-containing devices than for rGO-containing devices may accumulate at the QD layer and lead to the quenching of excitons, which is induced by the uplift of WF for GO with the ammonia reduction. In view of the photon energy of the QDs used in our devices ( $>2.0 \text{ eV}$ ,

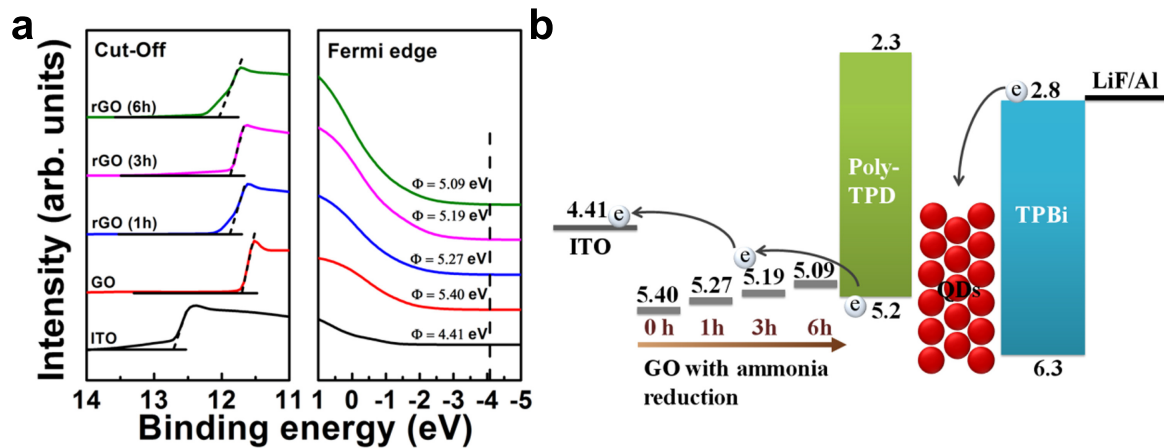


**Figure 4.** (a) UPS spectra of the ITO, GO coated on ITO, and GO with 1 h, 3 h, 6 h ammonia reduction coated on ITO. (b) The flat-band energy level diagram of the GO and rGO-based QLEDs.

obtained from the PL spectrum peak value of 617 nm), the  $V_{th}$  of all the fabricated devices is greater than the bandgap-voltage in our devices. However, because high charge density largely determines sub-bandgap  $V_{th}$  voltage due to Auger-assisted charge injection, we must consider that over-bandgap emission may be the result of high resistivity and low hole mobility of GO at over-bandgap drive voltages. Nevertheless, ammonia reduction can reduce resistivity and increase hole mobility of GO, which induces the decline of  $V_{th}$  for GO-containing devices. Figure 3(d) shows the current density–voltage characteristics of the QD-LEDs. The current density is increased with the ammonia reduced GO, among which Device d with 1 h ammonia reduction has the largest current density in comparison with other devices across the measurement range. This phenomenon can be attributed to the following two aspects: one is the enhancement of conductivity and hole mobility of GO after the ammonia reduction and the other is the enlargement of barrier to hole injection into the QDs with the uplift of WF for GO after the ammonia reduction, as further investigated below. These two effects jointly bring about the fact that device B has a larger current density than other GO or rGO-containing devices. Figure 3(e) shows current density–voltage for devices A–D plotted on double-logarithmic axes. Similar trap-limited conduction behavior is obtained in our devices by the Child’s law of  $J \propto V^m$ , as reported similarly elsewhere [28, 29]. The value of  $m$  is  $\sim 10.2$ ,  $\sim 8.8$ ,  $\sim 7.9$ , and  $\sim 7.8$  for devices A, B, C, and D, respectively. The  $m$  for the rGO-based devices is lower than that of GO-based device, indicating that the hole traps in the rGO film are fewer than those in the GO film. This may account for a higher current density in the rGO-based devices than that of the GO-based one.

Figure 3(f) shows the normalized EL spectra of the devices, which are slightly redshifted by 8–15 nm compared with the PL one. This redshift can be ascribed to the combined effect of both interdot interactions observed from closely packed QD solids and the electric-field-induced Stark effect. In addition, no parasitic emission from adjacent organic layers is observed in the EL spectra, which indicates

that the radiative recombination from the QDs dominates the emission of the devices.

To confirm the energy levels of GO and rGO, UPS spectra of the layers were recorded, as shown in figure 4(a). According to the difference between the inelastic cutoff and the Fermi edge, the WF values of ITO and GO-modified ITO can be calculated. After depositing the GO film onto the ITO, the WF increases from 4.41 eV to 5.40 eV, which agreed well with the previous report [25]. Nevertheless, when increasing the reduction time from 1 h to 6 h, the WF of rGO-modified ITO decreases from 5.27 eV to 5.09 eV. Therefore, we depict the energy level diagram of the QD-LEDs with different GO films as hole injection layers, as shown in figure 4(b). It is noteworthy that ammonia reduction brings about the improvement of WF values for GO, inducing large energy barriers between the hole injection layer and hole transport layer, which may decrease the formation of excitons in the QDs. However, compared to the difference in the WF values (0.99 eV) of ITO and GO, the improvement of WF values (0.31 eV) for GO appears to have a weak influence on hole injection from hole injection layer to the QD as ammonia reduction gives rise to the restoration of  $sp^2$  conjugation in the GO. In addition, as another important synergic factor, low resistivity of GO after ammonia reduction plays a crucial role in device performance, which can improve the charge transport and finally result in low  $V_{th}$  and high brightness. Moreover, the improvement of WF for GO will reduce the space charge accumulation at the QD layer and induce the rGO-containing devices to reach the peak efficiency at a low current density (figure S3). However, with the increase of ammonia-reduction time, the rGO layers perform rougher morphology as seen in the figure S4. Although further ammonia reduction will continuously enhance the conductivity and hole mobility of rGO, it also induces the increase of RMS in rGO layers, which will devastate the device performance on account of the larger leakage current and inefficient formation of excitons in the QDs. Finally, we confirm ammonia reduction for 1 h is most beneficial to the performance of GO-containing devices. Hence, tuning optical and electronic properties of charge transport or injection

layers is an important approach to optimize the performance of the QD-LEDs. Also, properly balancing the hole injection and transport can lead to the improved performance of QD-LEDs.

#### 4. Conclusions

In summary, we have rationally designed and realized fine-modulation on the optical and electronic properties of GO via ammonia reduction. The resultant rGO has been demonstrated to be a suitable hole injection layer for QD-LEDs. The rGO-based QD-LEDs show enhanced performance compared to the GO-based ones. We demonstrate that the QD-LED consisting of GO with 1 h ammonia reduction shows the best device performance (maximum luminance of  $936 \text{ cd m}^{-2}$ , and  $V_{\text{th}}$  of 5.0 V). The improved performance can be attributed to the synergistic effect of the improved conductivity ( $1.27 \mu\text{S cm}^{-1}$  versus  $0.139 \mu\text{S cm}^{-1}$ ) and decreased work function (5.27 eV versus 5.40 eV) of the GO. The results reported in this paper promise the use of graphene materials in high performance QD-LEDs.

#### Acknowledgments

This work was financially supported by the National Science Foundation for Distinguished Young Scholars of China (61425021); National Natural Science Foundation of China (11374296, and 61177040); China Postdoctoral Science Foundation (2015M582192); Startup Research Fund of Zhengzhou University (1512317006).

#### References

- [1] Colvin V L, Schlamp M C and Alivisatos A P 1994 *Nature* **370** 354
- [2] Zhao J L et al 2006 *Nano Lett.* **6** 463
- [3] Sun Q, Wang Y A, Li L, Wang D, Zhu T, Xu J, Yang C and Li Y 2007 *Nat. Photon.* **1** 717
- [4] Yu W W and Peng X 2002 *Angew. Chem., Int. Ed.* **41** 2368
- [5] Qian L, Zheng Y, Xue J and Holloway P H 2011 *Nat. Photon.* **5** 543
- [6] Shirasaki Y, Supran G J, Bawendi M G and Bulović V 2013 *Nat. Photon.* **7** 13
- [7] Rizzo A, Li Y Q, Kudera S, Della Sala F, Zanella M, Parak W J, Cingolani R, Manna L and Gigli G 2007 *Appl. Phys. Lett.* **90** 051106
- [8] Bae W K, Kwak J, Lim J, Lee D, Nam M K, Char K, Lee C and Lee S 2010 *Nano Lett.* **10** 2368
- [9] Bozyigit D, Yarema O and Wood V 2013 *Adv. Funct. Mater.* **23** 3024
- [10] Ji W Y, Jing P T, Zhao J L, Liu X Y, Wang Y Q and Li H B 2013 *Nanoscale* **5** 3474
- [11] Ji W Y, Jing P T and Zhao J L 2013 *J. Mater. Chem. C* **1** 470
- [12] Talapin D V, Lee J S, Kovalenko M V and Shevchenko E V 2010 *Chem. Rev.* **110** 389
- [13] Norrman K, Gevorgyan S A and Krebs F C 2009 *ACS Appl. Mater. Interfaces* **1** 102
- [14] Ji W Y, Lv Y, Jing P T, Zhang H, Wang J, Zhang H Z and Zhao J L 2015 *ACS Appl. Mater. Interfaces* **7** 15955
- [15] Ma H, Yip H L, Huang F and Jen A K-Y 2010 *Adv. Funct. Mater.* **20** 1371
- [16] Nardes A, Kemerink M, De Kok M, Vinken E, Maturova K and Janssen R 2008 *Org. Electron.* **9** 727
- [17] Norrman K, Madsen M V, Gevorgyan S A and Krebs F C 2010 *J. Am. Chem. Soc.* **132** 16883
- [18] Caruge J M, Halpert J E, Wood V, Bulović V and Bawendi M G 2008 *Nat. Photon.* **2** 247
- [19] Wood V, Panzer M J, Halpert J E, Caruge J M, Bawendi M G and Bulović V 2009 *ACS Nano* **3** 3581
- [20] Wood V, Panzer M J, Caruge J M, Halpert J E, Bawendi M G and Bulović V 2010 *Nano Lett.* **10** 24
- [21] Eda G, Mattevi C, Yamaguchi H, Kim H and Chhowalla M 2009 *J. Phys. Chem. C* **113** 15768
- [22] Mattevi C et al 2009 *Adv. Funct. Mater.* **19** 2577
- [23] Liu J, Xue Y H, Gao Y X, Yu D S, Durstock M and Dai L M 2012 *Adv. Mater.* **24** 2228
- [24] Yun J, Yeo J, Kim J, Jeong H, Kim D, Noh Y, Kim S, Ku B and Na S 2011 *Adv. Mater.* **23** 4923
- [25] Wang D Y, Wang I S, Huang I S, Yeh Y C, Li S S, Tu K H, Chen C C and Chen C W. 2012 *J. Phys. Chem. C* **116** 10181
- [26] Chen D Z, Li L D and Guo L 2011 *Nanotechnology* **22** 325601
- [27] Li D, Muller M B, Gilje S, Kaner R B and Wallace G G 2008 *Nat. Nanotechnol.* **3** 101
- [28] Xu W, Ji W Y, Jing P T, Yuan X, Wang Y A, Xiang W D and Zhao J L 2014 *Opt. Lett.* **39** 426
- [29] Dai X L, Zhang Z X, Jin Y Z, Niu Y, Cao H J, Liang X Y, Chen L W, Wang J P and Peng X G 2014 *Nature* **515** 96